AIAA-88-0624

CHOICE OF IMPLICIT AND EXPLICIT OPERATORS FOR THE UPWIND DIFFERENCING METHOD

Meng-Sing Liou
NASA Lewis Research Center
Cleveland, OH

Bram van Leer
The University of Michigan
Ann Arbor, MI
and
Institute for Computational Mechanics
in Propulsion (ICOMP)
NASA Lewis Research Center
Cleveland, OH

AIAA 26th Aerospace Sciences Meeting
January 11-14, 1988/Reno, Nevada

CHOICE OF IMPLICIT AND EXPLICIT OPERATORS
FOR THE UPWIND DIFFERENCING METHOD

Meng-Sing Liou*
NASA Lewis Research Center
Cleveland, Ohio
and
Bram van Leer†
The University of Michigan
Ann Arbor, Michigan

ABSTRACT

The flux-vector and flux-difference splittings of Steger-Warming, Van Leer and Roe are tested in all possible combinations in the implicit and explicit operators that can be distinguished in implicit relaxation methods for the steady Euler and Navier-Stokes equations. The tests include one-dimensional inviscid nozzle flow, and two-dimensional inviscid and viscous shock reflection. Roe's splitting, as anticipated, is found to uniformly yield the most accurate results. On the other hand, an approximate Roe splitting of the implicit operator (the complete Roe splitting is too complicated for practical use) proves to be the least robust with regard to convergence to the steady state. In this respect, the Steger-Warming splitting is the most robust: it leads to convergence when combined with any of the splittings in the explicit operator, although not necessarily in the most efficient way.

1. INTRODUCTION

Over the past five years conservative upwind differencing methods have been yielding

---

* Computational Fluid Dynamics Branch. Member AIAA.

† Department of Aerospace Engineering. Also: Institute for Computational
Mechanics in Propulsion (ICOMP), NASA Lewis Research Center, Cleveland, Ohio.
Member AIAA.

1

impressive results for compressible aerodynamics problems[1-4]. Among the techniques available for achieving the upwind bias the most prominent and most used ones are the flux-vector splittings (FVS) by Steger and Warming[5] and Van Leer[6], and the flux-difference splittings (FDS) by Roe[7] and Osher[8].

Until recently, most research efforts have been concentrated on implementing the different splitting formulas in the explicit operator by which the spatial residual is computed. With at least four methods to choose from, there clearly is a need for a shopping guide. Some comparisons have been made[2,9,10], from which the following conclusions can be drawn.

(i) Van Leer's flux-vector splitting by design and in practice is more accurate than Steger-Warming's, for both smooth and shocked flow[2].

(ii) Flux-vector splitting is less accurate than flux-difference splitting because it ignores contact discontinuities and shear waves. This inaccuracy particularly shows up as excessive numerical diffusion across a boundary layer[9,10].

Direct comparisons between Roe's and Osher's splittings are not known, but the methods should be very close in accuracy. There is a preference for the Roe splitting because of its algebraic simplicity, which makes its extension to real-gas physics straightforward[11], and its computational efficiency. For an ideal gas though, the Osher splitting can be coded almost as economically[12].

Little research has been devoted so far to the analysis and comparison of these splittings when used in the implicit iterative operators of implicit marching schemes. Particularly urgent are questions regarding their stability and convergence properties. Barth[12] performed a fixed-point analysis of some linearization of a fully implicit method for the one-dimensional Euler equations, incorporating either the exact or an approximate Jacobian matrix of Roe's splitting formula(hereafter referred to as RS and ARS respectively). Liou[14] made an eigenvalue analysis of the system resulting from the use of the true Jacobians of the Steger-Warming and Van Leer splittings(hereafter referred to as SWS and VLS respectively) in various relaxation procedures for the two-dimensional Euler equations.

The present paper addresses the following questions:

Is there an optimal combination of implicit and explicit upwind
operators, simultaneously achieving stability, accuracy and efficiency
for a wide class of problems?

The choice of splitting has been limited to the Steger-Warming, Van Leer and Roe splitting formulas. There is no need to use the same splitting in both implicit and explicit operators, so there are nine combinations to choose from. The following matters need special attention in this investigation.

(1) Uniqueness: it is not clear whether the same solution is obtained with different split fluxes because of their nonlinear nature. Specifically, one might ask if different implicit operators will drive toward the same solution if the same explicit operator is used.

(2) Sensitivity: the performance of the implicit operator may be sensitive to the changes of residual differencing accuracy, in particular from $O(\triangle x)$ to $O(\triangle x^2)$.

(3) Monotonicity: modern, monotonicity preserving(non-oscillatory) interpolation techniques for obtaining interface fluxes are known to affect convergence.

(4) Diffusivity: all splitting formulas ultimately are intended for the computation of the inviscid fluxes in the Navier-Stokes equations. The level of artificial diffusion in the explicit operator to a great extent determines the accuracy.

(5) Grid nonuniformity: grid stretching tends to slow down convergence; how this effect varies among the different flux formulas is not known.

The emphasis will be on (1),(2),(3) and (4). Items (4) and (5) often appear together in Navier-Stokes calculations, but it is important to understand their individual effects. These will only be briefly discussed here; a more detailed analysis is planned for the future.

It should be understood that the search for the optimum implicit method should not be limited to, and in fact, may very well lead outside the small set of splittings considered here. We think of this study only as a pathfinder for this search.

2. ANALYSIS

The stationary system of conservation laws for inviscid flows is written as

$$R(U) = \frac{\partial F}{\partial x} + \frac{\partial G}{\partial y} + \frac{\partial H}{\partial z} + S = 0, \tag{1}$$

where U is the vector of conserved state variables, i.e. $U = \rho(1, u, v, w, E)^T$; F, G, H are the corresponding inviscid fluxes and S is a source term. To make the nonlinear system numerically solvable, a Newton linearization procedure is employed, yielding the iterative equations

$$L(U)\delta U = -R(U), \tag{2a}$$

where

$$\delta U = U^{n+1} - U^n. \tag{2b}$$

$L(U)$ and $R(U)$ are called the implicit and the explicit operators respectively; the implicit operator is given by

$$L(U) = \frac{\partial}{\partial U}\left(\frac{\partial F}{\partial x} + \frac{\partial G}{\partial y} + \frac{\partial H}{\partial z} + S \right) = \frac{\partial R}{\partial U}. \tag{3}$$

Spatial discretizations of $L(U)$ and $R(U)$ are made using the upwind-differencing techniques of the FVS[5,6] and the FDS[7].

For an illustration, let us consider the x-flux F; the other two fluxes follow similarly. The Jacobian matrix A of F,

$$A = \frac{\partial F}{\partial U},$$ (4a)

is diagonalizable, with its right eigenvectors forming the columns of the transformation matrix Q:

$$A = Q^{-1}\Lambda Q, \qquad \Lambda = \text{diagonal matrix}.$$ (4b)

A splitting of Λ into nonnegative and nonpositive parts yields a splitting of A,

$$A^{\pm} = Q^{-}\Lambda^{\pm}Q,$$ (5a)

$$A = A^{+} + A^{-}.$$ (5b)

Steger and Warming[5] constructed the flux splitting

$$F = F^{+} + F^{-}$$ (6a)

by applying the eigenvalue splitting (5) and exploiting the fact that F is a homogeneous function of degree one. Hence the split fluxes and eigenvalues are connected by

$$F^{\pm} = \left(Q^{-1}\Lambda^{\pm}Q\right)U.$$ (6b)

The associated Jacobian matrices, often called true Jacobians, are denoted by

$$\tilde{A}^{\pm} = \frac{\partial F^{\pm}}{\partial U} \neq A^{\pm}.$$ (6c)

Unfortunately this splitting leads to discontinuous switching between F^{+} and F^{-}, that manifests itself in "glitches" at sonic and stagnation points, and broadening of shock profiles.

Van Leer[6] sought to remove this flaw by taking an entirely different approach. He devised a differentiable splitting of F in the form (6a) by writing the mass flux as the sum of two quadratic polynomials in Mach number, and building the momentum and energy fluxes on this basis. No requirement of homogeneity of the fluxes is needed. Recently a more general derivation has been presented[11], including a whole family of differentiable split fluxes and extending to a general equation of state for real gases.

Roe[7] constructed the flux-difference splitting by accounting for the wave interaction of neighboring cells via an approximate Riemann solution. He connected the difference in

fluxes with the difference in state variables by a "mean-value" Jacobian between neighboring states,

$$F_j - F_{j-1} = \bar{A}_{j-1/2}\left(U_j - U_{j-1}\right), \tag{7a}$$

$$\begin{aligned}
\bar{A}_{j-1/2} &\equiv A\left(U_{j-1}, U_j\right) \\
&= A\left(\bar{U}(U_{j-1}, U_j)\right) \\
&\equiv A\left(\bar{U}_{j-1/2}\right),
\end{aligned} \tag{7b}$$

where $\bar{A}$ is identical in form to A in (4a) but evaluated at the Roe-averaged state $\bar{U}$[7]. Again, eigenvalue splitting yields matrix splitting,

$$\bar{A}^{\pm} = \bar{Q}^{-1}\bar{\Lambda}^{\pm}\bar{Q}. \tag{8}$$

The eigenvalues of $\bar{A}$ vanish with the characteristic speeds in the x-direction or, in general, in the direction normal to the cell interface. This leads to a crisp representation of stationary discontinuity surfaces (shock, contact surface) when these are aligned with the interface.

With the above splittings, the implicit operator L contains the following nonzero contributions from the x-flux F:

$$FVS: \quad -\tilde{A}^{+}_{j-1}, \quad \left(\tilde{A}^{+}_{j} - \tilde{A}^{-}_{j}\right), \quad \tilde{A}^{-}_{j+1}, \tag{9a}$$

$$FDS: \quad -\frac{\partial}{\partial U_{j-1}}\left(\bar{A}^{+}_{j-1/2}U_{j-1}\right), \quad \frac{\partial}{\partial U_{j}}\left(\bar{A}^{+}_{j-1/2} - \bar{A}^{-}_{j+1/2}\right)U_j, \quad \frac{\partial}{\partial U_{j+1}}\left(\bar{A}^{-}_{j+1/2}U_{j+1}\right). \tag{9b}$$

The algebra involved in deriving the true Jacobians $\tilde{A}^{\pm}$ in the FVS is tedious; yet the algebra of differentiation in the FDS is formidable. Mulder and Van Leer[15] simplified the algebra considerably by ignoring the spatial derivatives of $\bar{A}^{\pm}$. The approximate form (referred to as ARS) yields the following elements in L:

$$ARS: \quad -\bar{A}^{+}_{j-1/2}, \quad \left(\bar{A}^{+}_{j-1/2} - \bar{A}^{-}_{j+1/2}\right), \quad \bar{A}^{-}_{j+1/2}. \tag{9c}$$

This approximation, as will be seen later, proves to be detrimental in some calculations.

For the discretization of the residual R let us denote the forward and backward difference operators by

$$\triangle^{+}(\bullet)_j = (\bullet)_{j+1} - (\bullet)_j,$$

$$\Delta^- (\bullet)_j = (\bullet)_j - (\bullet)_{j-1}. \tag{10a}$$

Then the approxiamtion of $\partial \mathbf{F}/\partial x$ is given in the compact form:

$$\frac{\partial \mathbf{F}_j}{\partial x} = \frac{1}{\Delta x}\left[\Delta^- \mathbf{F}_j^+ + \Delta^+ \mathbf{F}_j^- + \frac{\theta}{2}\Delta^+ \Delta^- (\mathbf{F}_{j-\ell}^+ - \mathbf{F}_{j+\ell}^-)\right] + O\left[\Delta x^{1+\theta}, \Delta x^2\right], \tag{10b}$$

which includes the following cases:

$$\theta = 0, \quad \text{first-order}$$
$$\theta = 1, \quad \text{second-order}$$

$$\ell = 1, \quad \text{full \quad upwinding}$$
$$\ell = 0, \quad \text{central \quad differencing.}$$

Note that for the evaluation of $\mathbf{L(U)}$ in (3) we always assume $\theta = 0$, while the $\mathbf{R(U)}$ has the option of taking $\theta = 0$ or $\theta = 1$. To eliminate oscillations and obtain a sharp representation of discontinuities, we use an upwind-based TVD scheme[16]. Equation (10b) may be modified by introducing a limiter φ multiplying the second-order flux differences.

$$\frac{\partial \mathbf{F}_j}{\partial x} = \frac{1}{\Delta x}\left[\Delta^- \mathbf{F}_j^+ + \Delta^+ \mathbf{F}_j^- + \frac{\theta}{2}\Delta^+ (\varphi_{j-1}\Delta^- \mathbf{F}_{j-\ell}^+ - \varphi_j\Delta^- \mathbf{F}_{j+\ell}^-)\right] + O\left[\Delta x^{1+\theta}, \Delta x^2\right]$$
$$\tag{10c}$$

The limiters are nonlinear functions of neighboring flux differences. For reasons mentioned in Section 4 we did not include this in the present study.

After substitution of spatial discretizations, along with proper treatment of boundary conditions given in next section, a block matrix system is obtained. To solve this system, direct LU decomposition is used for one-dimensional problems and line-relaxation procedures are used in the two-dimensional problems.

3. SPECIAL NUMERICAL PROCEDURES

In addition to what has been said in general about the numerical methods used, two special procedures must be discussed; these regard the entropy condition and various boundary conditions.

§3.1. Satisfying the Entropy Condition

Of all splitting methods described above, Roe's is the only one that may violate the entropy condition. This happens in particular in the case of a stationary expansion shock

6

located exactly at an interface. Just as for an admissible shock, the Roe matrix $\bar{A}$ has a vanishing eigenvalue. From the general flux formula,

$$
\begin{aligned}
\mathbf{F}_{j-1/2} &= \mathbf{F}_{j-1} + \bar{\mathbf{A}}_{j-1/2}^{-}(\mathbf{U}_j - \mathbf{U}_{j-1}) = \mathbf{F}_j - \bar{\mathbf{A}}_{j-1/2}^{+}(\mathbf{U}_j - \mathbf{U}_{j-1}) \\
&= \frac{1}{2}(\mathbf{F}_{j-1} + \mathbf{F}_j) - \frac{1}{2}|\bar{\mathbf{A}}_{j-1/2}|(\mathbf{U}_j - \mathbf{U}_{j-1}), \qquad |\mathbf{A}| \equiv \mathbf{A}^{+} - \mathbf{A}^{-},
\end{aligned}
\tag{11}
$$

it follows that the flux across the shock equals pre- and post-shock fluxes, and therefore can not cause any spreading of the wave. In practice, e.g. in the one-dimensional nozzle flows of Section 4.1, this leads to nonuniqueness of the numerical solution in the form of an expansion shock located at a sonic point. Its strength is a function of the precise path followed in reaching a steady state, and therefore depends on the implicit operator used (see Section 1, remark (1)). To overcome this problem one must make sure there is some residual dissipation. Following Harten[17] we do this by modifying the eigenvalues $|\lambda|$ of $|\mathbf{A}|$ when these are close to zero:

$$
|\lambda|_{j-1/2} \leftarrow \frac{(\lambda_{j-1/2}^2 + \epsilon_{j-1/2}^2)}{4\epsilon_{j-1/2}}, \qquad |\lambda_{j-1/2}| < \epsilon_{j-1/2},
\tag{12a}
$$

with

$$
\epsilon_{j-1/2} = K \max(\lambda_j - \lambda_{j-1}, 0), \qquad K > 0.
\tag{12b}
$$

This modification is needed only for the genuinely nonlinear characteristic families.

§3.2 Boundary Treatment

In order to achieve rapid convergence to the steady state, it is necessary to make the boundary procedure implicit. Explicit procedures will deteriorate the convergence rate and sometimes lead to instability. The question remains whether there is a unique and most effective implicit boundary procedure. The answer seems to be that there are perhaps as many boundary shemes in the literature as there are interior schemes. It also seems that even less definitive appraisals can be made of boundary schemes than of interior schemes. This may have the following causes: (1) Boundaries are only a small part of the whole domain considered, therefore one paid less attention; (2) There is a strong interaction between boundary and interior schemes, both on the level of the discretization and of the PDE itself. As Moretti[18] put it: "Flow evolution depends not only on the events at one boundary but on the interaction of the two boundaries and of the interior as well." The interaction is hard to analyze. Often a linear analysis can at best give clues as to the stability, but not at all to the convergence rate of the full method.

To compare the effect of the operators related to different split-flux formulas, it would seem reasonable to combine all with the same boundary treatment. This procedure obviously conflicts the statement (2) above and therefore may not lead to optimum results for

7

any of the interior schemes considered here. However, this is the best we can do, judging the present state of analysis. To illustrate our implicit boundary procedure, we consider subsonic outflow from a boundary point, denoted by subscript J. The static pressure is fixed, i.e.,

$$p_J = \text{const}, \tag{13a}$$

or

$$\triangle p_J = 0. \tag{13b}$$

This reduces to

$$\triangle(\rho E)_J = \left(u\triangle\rho u - \frac{1}{2}u^2\triangle\rho\right)_J. \tag{13c}$$

Allowing extrapolation of two variables from interior points, denoted by $J-1$ and $J-2$, we choose

$$\begin{pmatrix} \triangle\rho \\ \triangle\rho u \end{pmatrix}_J = (\alpha+1)\begin{pmatrix} \triangle\rho \\ \triangle\rho u \end{pmatrix}_{J-1} - \alpha\begin{pmatrix} \triangle\rho \\ \triangle\rho u \end{pmatrix}_{J-2}, \quad \alpha = 0 \text{ or } 1. \tag{14}$$

For the equation centered at $J-1$, the operator $L(U)$ has a term

$$\begin{aligned}
\mathbf{A}_J^-\triangle\mathbf{U}_J &= \begin{pmatrix} a_{11} & a_{12} & a_{13} \\ a_{21} & a_{22} & a_{23} \\ a_{31} & a_{32} & a_{33} \end{pmatrix}_J \begin{pmatrix} \triangle\rho \\ \triangle\rho u \\ u\triangle\rho u - \frac{1}{2}u^2\triangle\rho \end{pmatrix}_J \\
&= \begin{pmatrix} a_{11}\chi & a_{12}\beta & a_{13} \\ a_{21}\chi & a_{22}\beta & a_{23} \\ a_{31}\chi & a_{32}\beta & a_{33} \end{pmatrix}_J \begin{pmatrix} \triangle\rho \\ \triangle\rho u \\ 0 \end{pmatrix}_J \\
&= (\alpha+1)\begin{pmatrix} a_{11}\chi & a_{12}\beta & 0 \\ a_{21}\chi & a_{22}\beta & 0 \\ a_{31}\chi & a_{32}\beta & 0 \end{pmatrix}_J \begin{pmatrix} \triangle\rho \\ \triangle\rho u \\ \triangle\rho E \end{pmatrix}_{J-1} \\
&\quad - \alpha\begin{pmatrix} a_{11}\chi & a_{12}\beta & 0 \\ a_{21}\chi & a_{22}\beta & 0 \\ a_{31}\chi & a_{32}\beta & 0 \end{pmatrix}_J \begin{pmatrix} \triangle\rho \\ \triangle\rho u \\ \triangle\rho E \end{pmatrix}_{J-2},
\end{aligned} \tag{15}$$

where $\chi = (1 - \frac{1}{2}u^2)$ and $\beta = 1 + u$; the elements $(a_{11}, ..., a_{33})$ of $\mathbf{A}^-$ are known at J at the last iteration level. By substitution of (15) in the discrete equation centered at $J-1$, the boundary term $\mathbf{A}_J^-\triangle\mathbf{U}_J$ is now expressed in the interior terms $|\mathbf{A}_{J-1}|\triangle\mathbf{U}_{J-1}$ and $\mathbf{A}_{J-2}^+\triangle\mathbf{U}_{J-2}$. A similar procedure can be performed for a subsonic inflow boundary where we specify, as suggested by Yee et al[19],

$$\begin{aligned} \rho_1 &= \text{const}, \\ u_1 &= \text{const}. \end{aligned} \tag{16a}$$

Hence a spatial extrapolation to interior points gives

$$\Delta\rho E_1 = (\gamma - 1)^{-1}[(\alpha + 1)\Delta p_2 - \alpha\Delta p_3]$$

$$= (\alpha + 1)[\Delta\rho E - u\Delta\rho u + \frac{1}{2}u^2\Delta\rho]_2 \tag{16b}$$

$$- \alpha[\Delta\rho E - u\Delta\rho u + \frac{1}{2}u^2\Delta\rho]_3,$$

and $A_1^+ \Delta U_1$ yields contributions to the terms associated with ΔU_2 and ΔU_3.

As for supersonic inflow one simply sets

$$\Delta U_1 = 0, \tag{17}$$

and at the supersonic outflow boundary,

$$\Delta U_J = (\alpha + 1)\Delta U_{J-1} - \alpha\Delta U_{J-2}. \tag{18}$$

4. NUMERICAL TESTS

Numerical tests of the various combinations of implicit and explicit operators have been carried out for the Euler equations in one and two dimensions, and for the Navier-Stokes equations in two dimensions. The one-dimensional tests are nozzle-flow problems that are governed by the equations

$$\frac{\partial F}{\partial x} + S = 0, \tag{19a}$$

where the source term S includes the effect of nozzle area $s(x)$

$$S = \left(F - \begin{pmatrix} 0 \\ p \\ 0 \end{pmatrix}\right)\Phi(x), \qquad \Phi(x) = s'(x)/s(x). \tag{19b}$$

The area distribution for the divergent nozzle is given by

$$s(x) = 1.398 + 0.347\,tanh(0.8x - 4), \quad 0 \le x \le 10, \tag{20a}$$

and for the convergent-divergent nozzle by

$$s(x) = 1.75 - 0.75\,cos(x - 5)\pi/5, \quad 0 \le x \le 5$$
$$s(x) = 1.25 - 0.25\,cos(x - 5)\pi/5, \quad 5 \le x \le 10. \tag{20b}$$

9

Unless noted, 100 uniform meshes were used in the one-dimensional calculations.

The two-dimensional Euler problem concerns the reflection of a Mach 2.9 oblique shock wave off a solid surface at $y = 0$; the angle β between incident wave and wall is 29 degrees. The computational domain, $0 \leq x \leq 4$ and $0 \leq y \leq 1$, was equally divided into 60 by 20 meshes.

Finally, the Navier-Stokes calculation concerns the interaction of an oblique shock wave with a laminar boundary layer; the flow parameters are those of recent experiments[20] and are given later, along with details about the computational grid used.

§4.1 One-Dimensional Problems

For the one-dimensional nozzle problems, the variations in combinations of operators lead only to minor difference in accuracy and convergence rate if the flow is either fully supersonic or subsonic; these results therefore are not discussed in detail. Essential differences appear as a shock wave enters in the solution; the results are summarized in Tables 1 to 5 and Figures 1 to 4. Except for the changes in the flux formulas all calculations of the same flow were done for the same set of numerical parameters (grid spacing, relaxation factor) and with the same boundary treatment.This does not imply that any combination of operators achieves its peak performance. At this stage, our goal is merely to select a pair of operators that maintains stability, accuracy and reasonably fast convergence (say, within 100 iterations) for a wide range of problems. Once this goal has been reached one may start looking for ways to further improve the efficiency of the method.

Convergence is measured by summing up all changes in the state quantities:

$$\varepsilon = \sum_{grids} \sum_{\ell=1}^{3 \, or \, 4} |\delta U_\ell| \, ; \tag{21}$$

for a solution to be called "converged" ε must have been reduced to $O(10^{-11})$. The first set of results is for divergent-nozzle flow. Table 1 shows the error and number of iterations till convergence for all possible first-order and second-order accurate upwind approximation of $R(U)$; for $L(U)$ only the first-order approximations are used. To assure that convergence will be achieved at least for all first-order methods, an under-relaxation factor—varying in the range of 0.15 to 0.6—was applied in all Newton iterations. It is seen that the fastest convergence rate is generally achieved using Van Leer's splitting in $L(U)$, with approximate Roe's splitting (ARS) coming in second for first-order calculations of $R(U)$ but becoming totally useless in second-order calculations. In the latter case the iterations are led into a limit cycle.

The number of iterations needed appears to be lowest, regardless of the choice splitting in $L(U)$, when $R(U)$ is discretized with SWS. This may have to do with the fact that SWS

10

is the most dissipative of the three splittings considered. This dissipative effect is evident from Fig. 1; the SWS shock structure is clearly smeared on the subsonic side. The RS and VLS results are both excellent. Note that the results on the supersonic side of the shock are identical for all schemes, since the schemes are identical in that region and the solution is completely determined by the inflow conditions. Quantitative results are found in Table 2, where numerical values of the pressure, normalized by the point values of the exact solution, are listed.

In the second-order solutions of Fig.2 all flux formulas have produced a large overshoot of the Mach number in the pre-shock state; for SWS there is also a tendency to undershoot the post-shock state. This non-monotonicity could have been prevented by the introduction of limiters in the flux-differencing formula, as in (10c) (see [16] for details). It was found though that these limiters—nonlinear by design—have a strong effect on the convergence, always slowing it down and sometimes ending it in a limit cycle, although the error at which the limit cycle happens is far below the local discretization error. It thus appears that the effect of limiters should be studied separately; they have not been used in any of the one-dimensional calculations. Regardless of the performance near the shock, all second-order discretizations give better accuracy away from the shock than the first-order discretization, as evident from Table 2.

The convergent-divergent nozzle used for the next series of tests has a discontinuity in curvature at the throat, leading to a discontinuity in the first derivative of state variables. This makes it a good test of the accuracy of splittings. From Fig. 3 and 4 it is evident that in the area of accuracy, i.e. in $R(U)$, RS and VLS perform much better than SWS, which introduces an $O(\Delta x)$ jump at the sonic point.

Table 3 summarizes the convergence histories and indicates the need for consistency of $L(U)$ and $R(U)$. Invariably, a degradation of efficiency is observed when splittings are mixed. The worst matches are seen for SWS in $R(U)$, which can only be made to converge using SWS also in $L(U)$. In contrast, VLS and ARS/RS appear to be more or less interchangeable. While far from optimal, especially in the second-order case, SWS still seems to be most generally applicable splitting for use in $L(U)$. On the other hand, if one would preclude SWS in $R(U)$ for its inaccuracy, the choice for $L(U)$ clearly belongs to VLS.

In order to further study the applicability of SWS as a multi-purpose splitting in $L(U)$ we removed the under-relaxation factor for the Newton iteration, allowing each scheme to converge at the maximum possible rate. With the same splitting and the same accuracy in $L(U)$ and $R(U)$, quadratic convergence may be achieved. The results for the divergent nozzle are listed in Table 4. Quadratic convergence is indeed observed for SWS/SWS and VLS/VLS with first-order accuracy; these are the only combinations that form a true Newton method. The general applicability of SWS in $L(U)$ is evident; without

under-relaxation VLS or ARS in L(U) can not be mixed with another splitting in R(U). Second-order accuracy with RS in R(U) can not even be obtained with ARS as the implicit driver, while SWS accomplishes this without any problem(see remark(2) in Section 1).

A final experiment, this time for the convergent-divergent nozzle, was to double Δx and observe the effect on convergence and stability. The results are compiled in Table 5; these show no significant changes with respect to those in Table 3.

From these one-dimensional experiments we may draw some provisional conclusions.

Regarding the implicit operator:
(1) SWS is prefered over VLS and ARS as a general technique, because of its robustness. It is applicable, even without under-relaxation, with each of the splittings used in the explicit operator, and achieves convergence—even with second-order approximation of R(U)—within 100 iterations.
(2) Implicit VLS combined with explicit VLS leads to the best convergence rate, even for the second-order explicit operator.
(3) ARS in the form (9c) is not an acceptable implicit discretization, not even in combination with explicit RS. The subject of approximating the Jacobian of Roe's flux clearly needs futher study.

Regarding the explicit operator:
(1) RS and VLS are far superior to SWS regarding the numerical accuracy achieved; it may be noted that VLS requires fewer operations than RS.

From the above conclusions one may further derive that VLS used in both implicit and explicit operators is a "best buy" as to the accuracy and convergence rate achieved in the one-dimensional nozzle problems. When comparing the above conclusions with (i) and (ii) in Section 1, we have not yet been able to make a clear distinction in accuracy between VLS and RS. This is due to the absence of a contact discontinuity in the one-dimensional test problems. This issue will be resolved by the Navier-Stokes experiment of Section 4.3.

§4.2 Two-Dimensional Euler Problem

For the shock-reflection problem we may allow ourselves to concentrate on accuracy. Owing to the flow being fully supersonic in the x-direction, convergence is achieved within eight iterations for all schemes using line/Gauss-Seidel relaxation with the line in the y-direction and downstream sweeping in the x-direction. The other side of the coin is that the upwind schemes lose their property of representing a shock front by a narrow profile. This is illustrated by Fig. 5, showing the pressure distribution on the wall ($y = 0$) and at the mid-plane ($y = 0.5$), with RS and first-order accuracy. When going to second-order accuracy, resolution is greatly improved, as shown in Fig. 6; there is hardly any difference between using RS or VLS in R(U). (SWS was dropped as a discretization for R(U)

12

because of its inferior performance in the tests of Section 4.1) The pressure undershoots and overshoots near the shocks can be avoided by using the limiters, see (10c), as is illustrated by Fig. 7. There is a large choice of limiters[21]; here we used the "minmod" function for illustration. Wall pressures from the first-order and second-order solutions are also tabulated in Table 5.

Although other limiters—for example "superbee"—may sharpen the shock profile, it should be noted that any genuine improvement of the representation of oblique shocks in supersonic flow must involve either grid adaptation or some kind of wave-recognition algorithm[22].

As anticipated, the results of the above two-dimensional Euler tests do not add anything to the results of the one-dimensional tests in regard to discriminating between VLS and RS.

§4.3 Two-Dimensional Navier-Stokes Problem

As for the Navier-Stokes calculations, we again concentrate on the issue of accuracy. The SWS is assumed an acceptable driver in $L(U)$ while $R(U)$ is varied according to the three flux formulas. The thin-layer form of the Navier-Stokes equations results in these operators:

$$R(U, U_y) = \frac{\partial F}{\partial x} + \frac{\partial G}{\partial y} - \frac{\partial W}{\partial y} = 0, \qquad (22a)$$

where F and G are again the inviscid fluxes and W is the viscous flux that involves only the y-derivatives

$$W(U, U_y)^T = \frac{\gamma M_\infty^2 \mu}{Re_\infty} \left[0, \frac{\partial u}{\partial y}, \frac{4}{3}\frac{\partial v}{\partial y}, u\frac{\partial u}{\partial y} + \frac{4v}{3}\frac{\partial v}{\partial y} + \frac{\gamma}{P_r}\frac{\partial e}{\partial y} \right],$$

and

$$L(U) = \frac{\partial}{\partial x}\left(\frac{\partial F}{\partial U}\delta U\right) + \frac{\partial}{\partial y}\left(\frac{\partial G}{\partial U}\delta U\right) - \frac{\partial^2}{\partial y^2}\left(\frac{\partial W}{\partial U_y}\delta U\right). \qquad (22b)$$

A detailed description of the derivation and the resulting algebraic system can be found in [23]. While the convective terms continue to be upwind-differenced, but the diffusion terms are now central-differenced because the latter have no bias in direction.

To minimize the uncertainties regarding turbulence modeling in the tests, we restrict ourselves to laminar flow. The problem chosen for tests is the interaction of an oblique shock wave with a boundary layer over a flat plate, recently reported in [20]. The flow parameters are: $M_\infty = 2.2, R_{e\infty} = 1.0 \times 10^5$, and the wedge angle of 3.75 degrees producing a shock angle of 30.027 degrees; the reference length used in Re_∞ is the distance from the

13

leading edge to the point of shock inpimgement on the plate. The wall is adiabatic, the Prandtl number is 0.72 and the viscosity is assumed to follow Sutherland's formula.

It was found in [23] that a grid distribution deduced from the triple-deck theory[24] gave results more accurate than those not based on such a grid[25]. Here we again use the same spacing,

$$
\begin{cases}
\Delta x = 0.03, \\
\Delta y_i = 1.5625e(-4), & 1 \leq i \leq 4, \\
\Delta y_i = 1.1868\Delta y_{i-1}, & 5 \leq i \leq 33, \\
\Delta y_i = 3.75e(-2), & i > 33;
\end{cases}
\tag{23}
$$

the total number of meshes is 75×65. The co-ordinates x and y have been non-dimensionalized by the same reference length for Re_∞.

The flow remains supersonic on all boundaries except at and near the wall. The computational domain is chosen such that the reflected shock wave from the wall does not intersect the top boundary and the flow is sufficiently well-developed after leaving the interaction region. Hence it is appropriate to specify all variables at the inflow and the top boundaries. Linear extrapolation from the interior points is used for the variables at the outflow.

In [23] only SWS was used; at present we also include the other splittings for comparison. Figure 8 shows the calculated and measured surface pressure; Roe's splitting is clearly more accurate than the Van Leer and Steger-Warming splittings which tend to diffuse details of the solution (see Section 1, remark (4)). Convergence also happens to be fastest with RS, taking about 250 iterations as compared to 400 for VLS and 520 for SWS for ε to be reduced by five orders of magnitude. It is worth mentioning that the present upwind-differencing results are much closer to the data than the central-differencing results in [20]. Also the convergence is faster using Roe's scheme although it needs slightly more computations in each iteration.

5. CONCLUSIONS

The present study confirms some previously known results regarding the accuracy of various splitting algorithms, and adds some regarding their use in implicit operators. As to the question of accuracy, Roe's flux-difference splitting clearly is superior to the two flux-vector splittings considered—Van Leer's and Steger-Warming's—and should be considered the best choice for use in a Navier-Stokes code. If only Euler calculations are considered and contact discontinuities or vortex sheets are not important, Van Leer's splitting is an attractive alternative. All splittings give insufficient resolution of an oblique shock wave in supersonic flow.

As to convergence, the Steger-Warming splitting is the only splitting of the *implicit* operator that can be combined with any of the splittings of the explicit operators and may therefore called the most robust of all splittings. This conclusion is of limited importance, since accuracy requirements clearly exclude the use of the Steger-Warming splitting in the *explicit* operator. Under this constraint, the Van Leer splitting becomes the better splitting for the implicit operator, since it leads to faster convergence with the remaining splittings of the explicit operator. The data, however, are inconclusive, since a Navier-Stokes computation with the Van Leer splitting as the implicit operator is yet missing.

Least effective on the implicit side is the approximate Roe splitting, which in second-order calculations even fails to lead to convergence in combination with the Roe splitting on the explicit side. It must be mentioned that the approximate Roe splitting, precisely because it is approximate, is not unique; many variations may have to be tested separately.(Barth[13] considers two and explains their different behavior in earlier and later stages of convergence.) This situation is far from desirable, but the use of the exact Jacobian of the Roe splitting in the implicit operator is even less attractive, because of its great computational cost.

Future extensions of the present study will concentrate on the question of selecting for the discretized Navier-Stokes equations a splitting of the implicit operator that is efficient and robust when combined with the Roe splitting of the explicit (residual) operator.

REFERENCES

1. Osher, S. and Chakravarthy, S., "Upwind Schemes and Boundary Conditions with Applications to Euler Equations in General Geometries," *Journal of Computational Physics,* Vol. 50, 1983, pp.447-481.
2. Anderson, W.K., Thomas, J.L. and Van Leer, B., "Comparison of Finite-Volume Flux-Vector Splittings for the Euler Equations," *AIAA Journal,* Vol. 24, 1986, pp.1453-1460.
3. Moon, Y.J. and Yee, H.C., "Numerical Simulation by TVD Schemes of Complex Shock Reflections from Airfoils at High Angle of Attack," AIAA paper 87-0350, 1987.
4. Lytton, C.C., "Solution of the Euler Equations for Transonic Flow over a Lifting Aerofoil-The Bernoulli Formulation (Roe/Lytton Method)," *Journal of Computational Physics*, Vol. 73, 1987, pp.395-431.
5. Steger, J.L. and Warming, R.F., "Flux Vector Splitting of the Inviscid Gasdynamics Equations with Application to Finite Difference Methods," *Journal of Computational Physics*, Vol. 40, 1981, pp.263-293.
6. Van Leer, B., "Flux-Vector Splitting for the Euler Equations," *Lecture Notes in Physics*, Vol. 170, 1982, pp.507-512.

7. Roe, P.L., "Approximate Riemann Solvers, Parameter Vectors, and Difference Schemes," *Journal of Computational Physics*, Vol. 43, 1981, pp.357-372.

8. Osher, S., "Numerical Solution of Singular Perturbation Problems and Hyperbolic Systems of Conservation Laws," North-Holland *Mathematical Studies*, Vol. 47, 1981, pp.179-205.

9. Koren, B., "Upwind Schemes for the Navier-Stokes Equations," Contributed paper, Second International Conference on Hyperbolic Equations, Aachen, March 14-18, 1988.

10. Van Leer, B., Thomas, J.L., Roe, P.L., and Newsome, R.W., "A Comparison of Numerical Flux Formulas for the Euler and Navier-Stokes Equations," AIAA paper 87-1104-CP, 1987.

11. Liou, M.-S., Van Leer, B. and Shuen, J.-S., "Splitting of Inviscid Fluxes for Real Gases," Contributed paper, First National Fluid Dynamics, Cincinnatti, OH, July 24-28, 1988.

12. Spekreijse, S.P., "Multigrid Solution of the Steady Euler Equations," Thesis, Center for Mathematics and Computer Science, Amsterdam, 1987.

13. Barth, T.J., "An Analysis of Implicit Local Linearization Techniques for Upwind and TVD algorithms," AIAA paper 87-0595, 1987.

14. Liou, M.-S., "Eigenvalue Analysis of Implicit Upwind Relaxation Schemes Using Flux-Vector Splittings," in preparation.

15. Mulder, W.A. and van Leer, B., "Experiments with Implicit Upwind Methods for the Euler Equations," *Journal of Computational Physics*, Vol. 59, 1985, pp.232-246.

16. Liou, M.-S., "A Generalized Procedure for Constructing an Upwind-Based TVD Schemes", AIAA paper 87-0355, 1987.

17. Harten, A., "High Resolution Schemes for Hyperbolic Conservation Laws," New York University Report DOE/ER/03077-167, 1982.

18. Moretti, G., "A Physical Approach to the Numerical Treatment of Boundaries in Gas Dynamics," in: Numerical Boundary Condition Procedures, NASA CP 2201, 1981.

19. Yee, H.C., Beam, R.M. and Warming, R.M., "Boundary Approximations for Implicit Schemes for One-Dimensional Inviscid Equations of Gasdynamics," *AIAA Journal*, Vol 20, 1982, pp.1203-1211.

20. Degrez, G., Boccadoro, C.H. and Wendt, J.F., "The Interaction of an Oblique Shock Wave with a Laminar Boundary Layer Revisited. An Experimental and Numerical Study," *Journal of Fluid Mechanics*, Vol. 177, 1987, pp.247-263.

21. Roe, P.L., "Characteristic-Based Schemes for the Euler Equations," *Annual Review of Fluid Mechanics*, Vol. 18, 1986, pp.337-365.

22. Van Leer, B., "The Computation of Steady Solutions to the Euler Equations: A Perspective," in: *Proceedings of the GAMM Workshop on the Numerical Simulation of Compressible Flows,*" Vieweg, Braunschweig, to appear.

16

23. Liou, M.-S., "An Efficient Navier-Stokes Solution of Shock Wave/Boundary Layer Interactions," Fifth International Conference on Numerical Methods in Laminar and Turbulent Flow, Montreal, Canada, July 6-10, 1987. Also submitted for publication.
24. Stewartson, K. and Williams, P.G., 'Self-induced separation,' *Proc. R. Soc. London Ser. A,* Vol. 312, 1969, pp.181-206.
25. Thomas, J.L. and Walters, R.W., 'Upwind relaxation algorithms for the Navier-Stokes Equations," *AIAA Journal,* Vol. 25, 1987, pp.527-534.
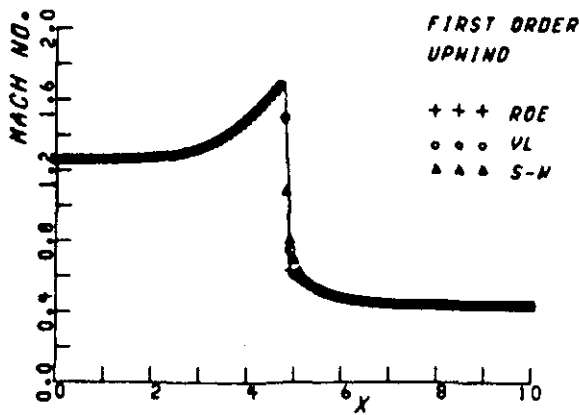
Figure 1. Divergent nozzle, $M_\infty = 1.26, P_e/P_t = 0.746$; first-order accurate $R(U)$. Solid line: exact solution, symbols: numerical solution.
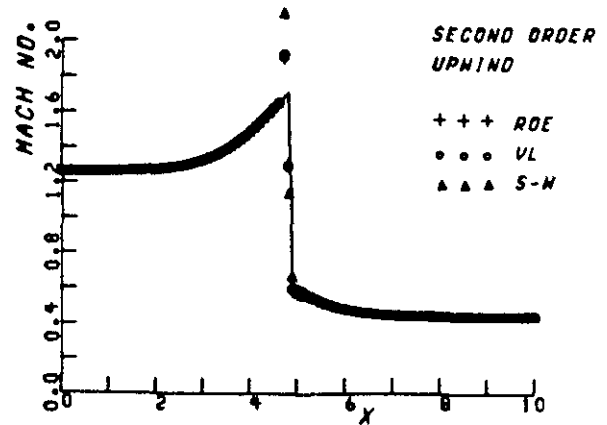

Figure 2. Divergent nozzle, $M_\infty = 1.26, P_e/P_t = 0.746$; second-order accurate $R(U)$. Solid line: exact solution, symbols: numerical solution.

Table 1

Convergence of numerical solutions for a divergent nozzle flow;
$M_\infty = 1.26, P_e/P_t = 0.746$. The maximum number of
iteration allowed was 300.

L(U)	R(U)	$O(\Delta x)$		$O(\Delta x^2)$	
		Error	No. of iter.	Error	No. of iter.
SWS	SWS	6.692(-11)	67	6.635(-11)	112
	VLS	7.828(-11)	118	8.230(-11)	127
	RS	8.786(-11)	120	8.576(-11)	127
VLS	SWS	6.676(-11)	68	6.297(-11)	106
	VLS	8.836(-11)	75	7.233(-11)	105
	RS	7.929(-11)	81	8.881(-11)	105
ARS	SWS	7.262(-11)	75	––	–––
	VLS	9.087(-11)	93	––	–––
	RS	7.325(-11)	94	––	––

––Stagnant or slow convergence

Table 2
Ratio of numerical to exact solutions for a divergent nozzle flow;
$M_\infty = 1.26, P_e/P_t = 0.746.$

| X	P_{comp}/P_{exact}					
	$O(\Delta x)$			$O(\Delta x^2)$		
	SWS	VLS	RS	SWS	VLS	RS
4.0	0.98583(0)	0.98583(0)	0.98583(0)	0.99944(0)	0.99944(0)	0.99944(0)
4.1	0.98528(0)	0.98528(0)	0.98528(0)	0.99953(0)	0.99953(0)	0.99953(0)
4.2	0.98489(0)	0.98489(0)	0.98489(0)	0.99964(0)	0.99964(0)	0.99964(0)
4.3	0.98467(0)	0.98467(0)	0.98467(0)	0.99977(0)	0.99977(0)	0.99977(0)
4.4	0.98465(0)	0.98465(0)	0.98465(0)	0.99992(0)	0.99992(0)	0.99992(0)
4.5	0.98485(0)	0.98485(0)	0.98485(0)	0.10001(1)	0.10001(1)	0.10001(1)
4.6	0.98527(0)	0.98527(0)	0.98527(0)	0.10003(1)	0.10003(1)	0.10003(1)
4.7	0.10445(1)	0.98593(0)	0.98593(0)	0.66515(0)	0.81497(0)	0.82237(0)
4.8	0.21495(1)	0.15310(1)	0.14962(1)	0.17969(1)	0.14880(1)	0.14924(1)
4.9	0.80460(0)	0.94106(0)	0.98479(0)	0.94302(0)	0.10412(1)	0.10530(1)
5.0	0.88994(0)	0.98294(0)	0.98751(0)	0.10384(1)	0.10144(1)	0.10002(1)
5.1	0.93628(0)	0.98412(0)	0.98850(0)	0.10241(1)	0.99985(0)	0.99979(0)
5.2	0.95951(0)	0.98534(0)	0.98947(0)	0.10035(1)	0.99980(0)	0.99982(0)
5.3	0.97113(0)	0.98657(0)	0.99043(0)	0.99769(0)	0.99979(0)	0.99981(0)
5.4	0.97740(0)	0.98779(0)	0.99135(0)	0.99851(0)	0.99978(0)	0.99980(0)
5.5	0.98126(0)	0.98897(0)	0.99223(0)	0.99965(0)	0.99979(0)	0.99980(0)
5.6	0.98401(0)	0.99011(0)	0.99307(0)	0.99995(0)	0.99980(0)	0.99981(0)
5.7	0.98620(0)	0.99118(0)	0.99385(0)	0.99991(0)	0.99981(0)	0.99982(0)
5.8	0.98803(0)	0.99218(0)	0.99456(0)	0.99987(0)	0.99983(0)	0.99983(0)
5.9	0.98962(0)	0.99310(0)	0.99522(0)	0.99987(0)	0.99984(0)	0.99984(0)
6.0	0.99101(0)	0.99394(0)	0.99581(0)	0.99988(0)	0.99986(0)	0.99986(0)
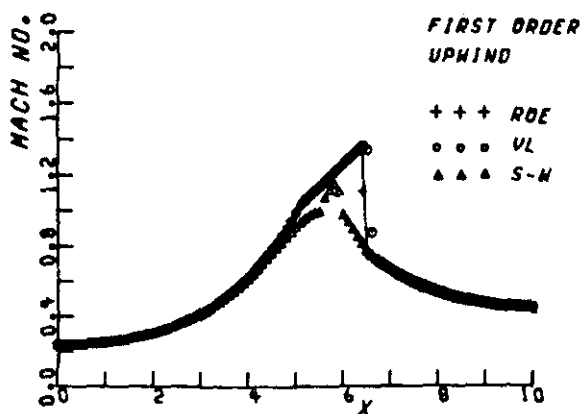
Figure 3. Convergent-divergent nozzle, $M_\infty = 0.2395$, $P_e/P_t = 0.84$; first-order accurate R(U). Solid line: exact solution, symbols: numerical solution.

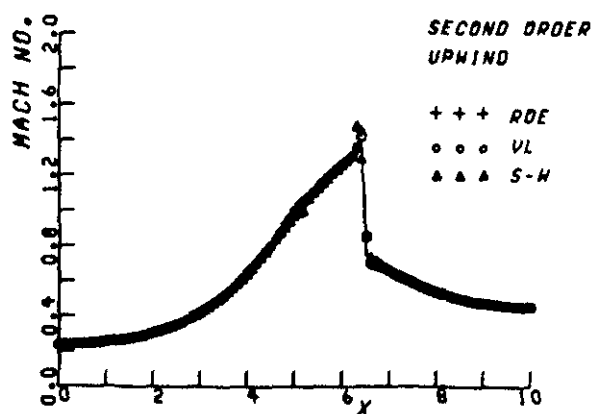Figure 4. Convergent-divergent nozzle, $M_\infty = 0.2395$, $P_e/P_t = 0.84$; second-order accurate R(U). Solid line: exact solution, symbols: numerical solution.

Table 3
Convergence of numerical solutions for a convergent-divergent
nozzle flow; $M_\infty = 0.2395, P_e/P_t = 0.84$.

L(U)	R(U)	$O(\Delta x)$		$O(\Delta x^2)$	
		Error	No. of iter.	Error	No. of iter.
SWS	SWS	8.419(-11)	189	8.325(-11)	187
	VLS	2.068(-06)	300	1.695(-06)	300
	RS	3.030(-10)	300	1.944(-06)	300
VLS	SWS	— —	— —	— —	— —
	VLS	8.542(-11)	204	9.034(-11)	176
	RS	6.857(-08)	300	7.002(-11)	175
ARS	SWS	— —	— —	— —	— —
	VLS	4.661(-08)	300	6.922(-08)	300
	RS	8.719(-11)	189	9.290(-11)	200

— —Stagnant or slow convergence

Table 4
Improvement of convergence rate for a divergent nozzle flow; $M_\infty = 1.26, P_e/P_t = 0.746$.

L(U)	R(U)	$O(\Delta x)$		$O(\Delta x^2)$	
		Error	No. of iter.	Error	No. of iter.
SWS	SWS	8.464(-11)	23	8.911(-11)	63
	VLS	7.688(-11)	45	5.139(-11)	79
	RS	6.907(-11)	45	6.776(-11)	79
VLS	VLS	5.594(-11)	23	5.682(-11)	59
ARS	RS	6.846(-11)	46	--	--

——Unstable, also for other pairs not listed.

Table 5
Effect of doubling Δx on convergence of numerical solutions for a convergent-devergent nozzle flow; $M_\infty = 0.2395, P_e/P_t = 0.84$.

L(U)	R(U)	$O(\Delta x)$		$O(\Delta x^2)$	
		Error	No. of iter.	Error	No. of iter.
SWS	SWS	9.118(-11)	159	9.280(-11)	211
	VLS	4.012(-06)	300	3.082(-06)	300
	RS	1.987(-06)	300	1.180(-06)	300
VLS	SWS	--	--	--	--
	VLS	7.324(-11)	192	8.868(-11)	176
	RS	8.289(-11)	189	9.843(-11)	179
ARS	SWS	--	--	--	--
	VLS	1.962(-07)	300	3.761(-07)	300
	RS	1.601(-06)	300	1.180(-11)	221

——Stagnant or slow convergence
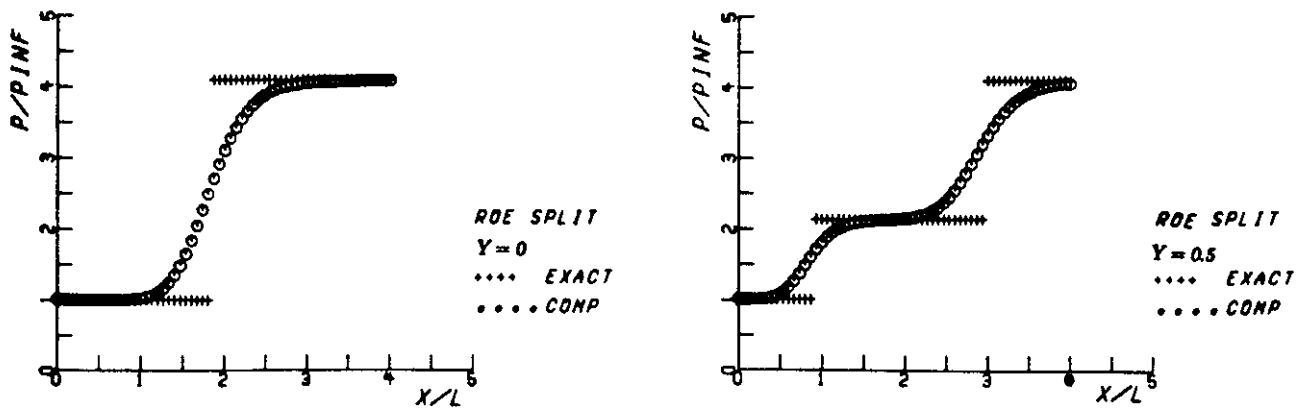
Figure 5. Shock reflection problem, $M_\infty = 2.9, \beta = 29°$;
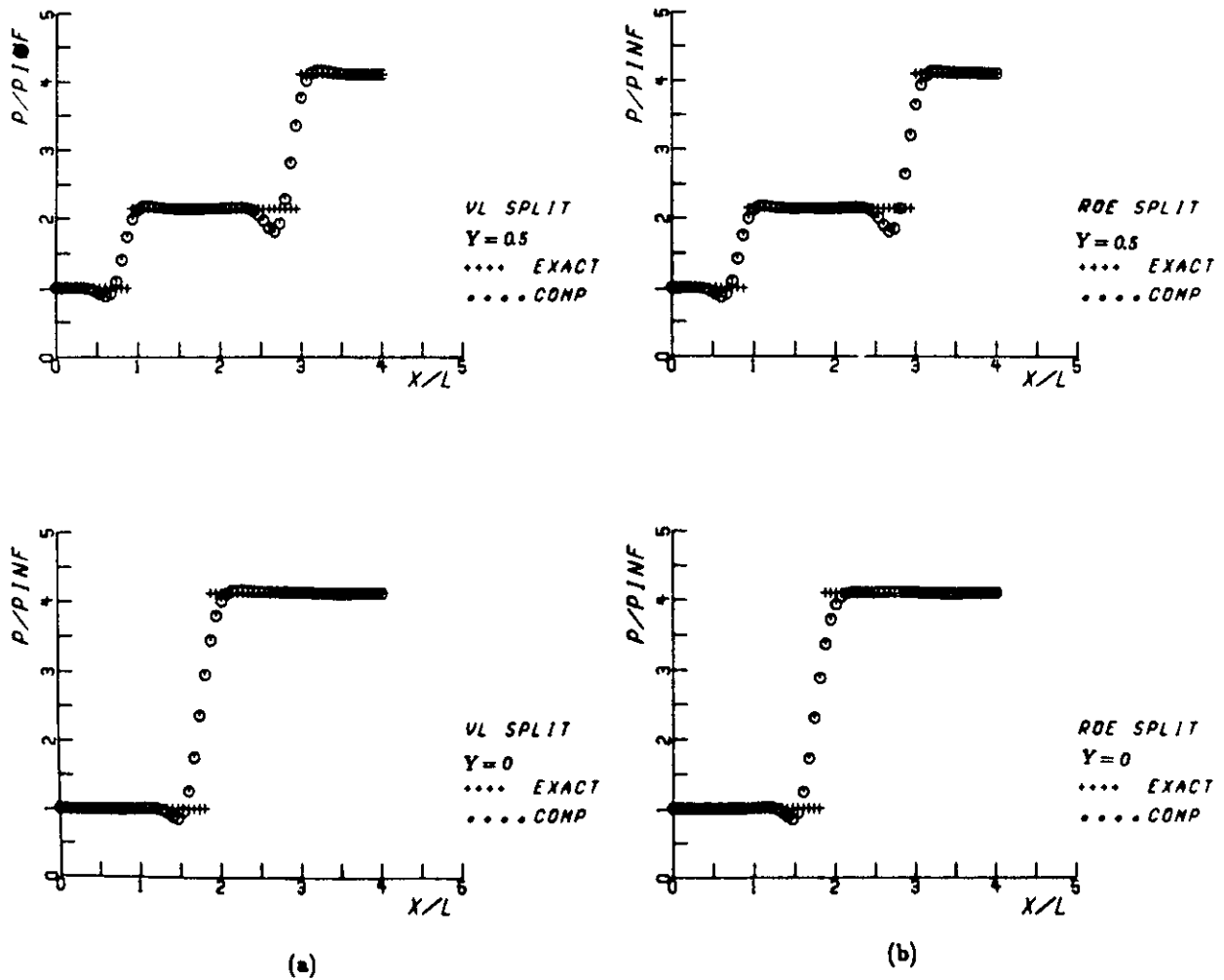first-order accurate R(U) using RS; +++: exact
solution, ○○○: numerical solution.

(a)   (b)

Figure 6. Shock reflection problem, $M_\infty = 2.9, \beta = 29°$;
second-order accurate R(U) using (a) VLS and (b)
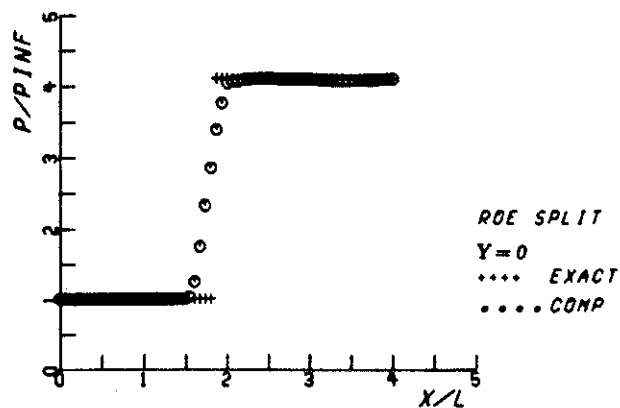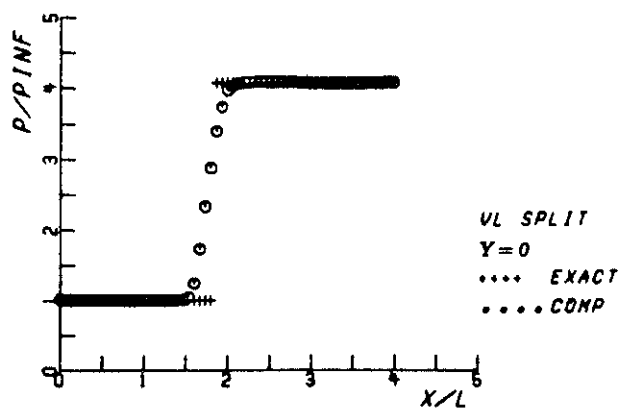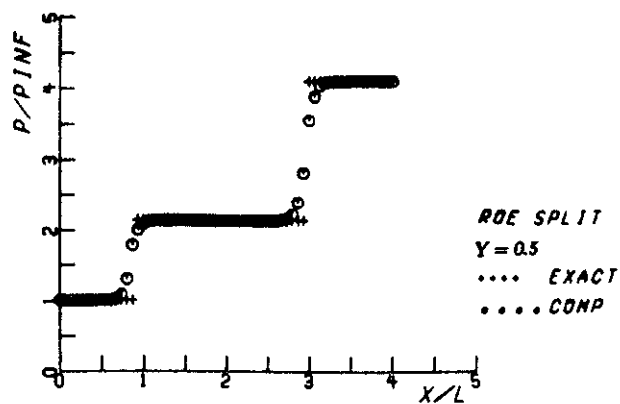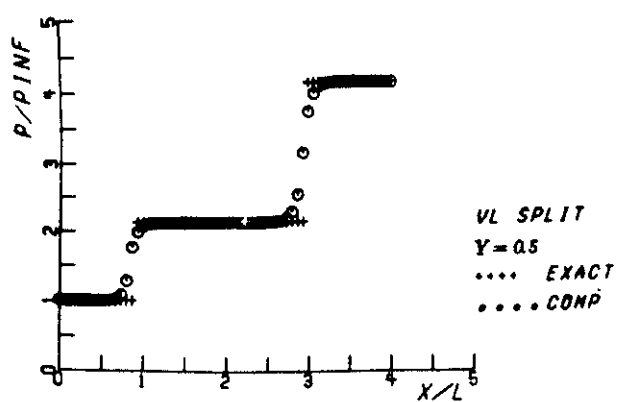RS; +++: exact solution, ○○○: numerical solution.

Figure 7. Shock reflection problem, $M_{\infty} = 2.9, \beta = 29°$; second-order accurate TVD R(U) using (a) VLS and (b) RS; +++: exact solution, o o o: numerical solution.

Table 6
Comparison of numerical and exact solutions for a
shock reflection problem; $M_\infty = 2.90, \beta = 29.0°$.

| X	Exact	$O(\Delta x^2)$		TVD	
		VLS	RS	VLS	RS
1.000	0.1000(1)	0.1007(1)	0.1007(1)	0.1000(1)	0.1000(1)
1.067	0.1000(1)	0.1012(1)	0.1012(1)	0.1000(1)	0.1000(1)
1.133	0.1000(1)	0.1013(1)	0.1015(1)	0.1000(1)	0.1000(1)
1.200	0.1000(1)	0.1006(1)	0.1011(1)	0.1000(1)	0.1000(1)
1.267	0.1000(1)	0.9843(0)	0.9912(0)	0.1000(1)	0.1000(1)
1.333	0.1000(1)	0.9447(0)	0.9501(0)	0.1001(1)	0.1000(1)
1.400	0.1000(1)	0.8886(0)	0.8862(0)	0.1003(1)	0.1001(1)
1.467	0.1000(1)	0.8578(0)	0.8430(0)	0.1010(1)	0.1004(1)
1.533	0.1000(1)	0.9534(0)	0.9343(0)	0.1048(1)	0.1031(1)
1.600	0.1000(1)	0.1252(1)	0.1237(1)	0.1248(1)	0.1246(1)
1.667	0.1000(1)	0.1742(1)	0.1725(1)	0.1744(1)	0.1750(1)
1.733	0.1000(1)	0.2342(1)	0.2309(1)	0.2353(1)	0.2324(1)
1.800	0.1000(1)	0.2936(1)	0.2885(1)	0.2896(1)	0.2852(1)
1.867	0.4108(1)	0.3429(1)	0.3370(1)	0.3425(1)	0.3392(1)
1.933	0.4108(1)	0.3778(1)	0.3720(1)	0.3766(1)	0.3761(1)
2.000	0.4108(1)	0.3988(1)	0.3938(1)	0.4005(1)	0.4045(1)
2.067	0.4108(1)	0.4095(1)	0.4052(1)	0.4065(1)	0.4070(1)
2.133	0.4108(1)	0.4138(1)	0.4099(1)	0.4094(1)	0.4077(1)
2.200	0.4108(1)	0.4147(1)	0.4113(1)	0.4110(1)	0.4090(1)
2.267	0.4108(1)	0.4144(1)	0.4114(1)	0.4117(1)	0.4103(1)
2.333	0.4108(1)	0.4137(1)	0.4112(1)	0.4120(1)	0.4106(1)
2.400	0.4108(1)	0.4130(1)	0.4112(1)	0.4120(1)	0.4110(1)
2.467	0.4108(1)	0.4125(1)	0.4114(1)	0.4119(1)	0.4111(1)
2.533	0.4108(1)	0.4122(1)	0.4116(1)	0.4118(1)	0.4110(1)
2.600	0.4108(1)	0.4121(1)	0.4118(1)	0.4117(1)	0.4108(1)
2.667	0.4108(1)	0.4119(1)	0.4120(1)	0.4115(1)	0.4104(1)
2.733	0.4108(1)	0.4118(1)	0.4120(1)	0.4113(1)	0.4103(1)
2.800	0.4108(1)	0.4116(1)	0.4119(1)	0.4111(1)	0.4103(1)
2.867	0.4108(1)	0.4114(1)	0.4117(1)	0.4108(1)	0.4104(1)
2.933	0.4108(1)	0.4111(1)	0.4114(1)	0.4105(1)	0.4104(1)
3.000	0.4108(1)	0.4109(1)	0.4111(1)	0.4102(1)	0.4104(1)
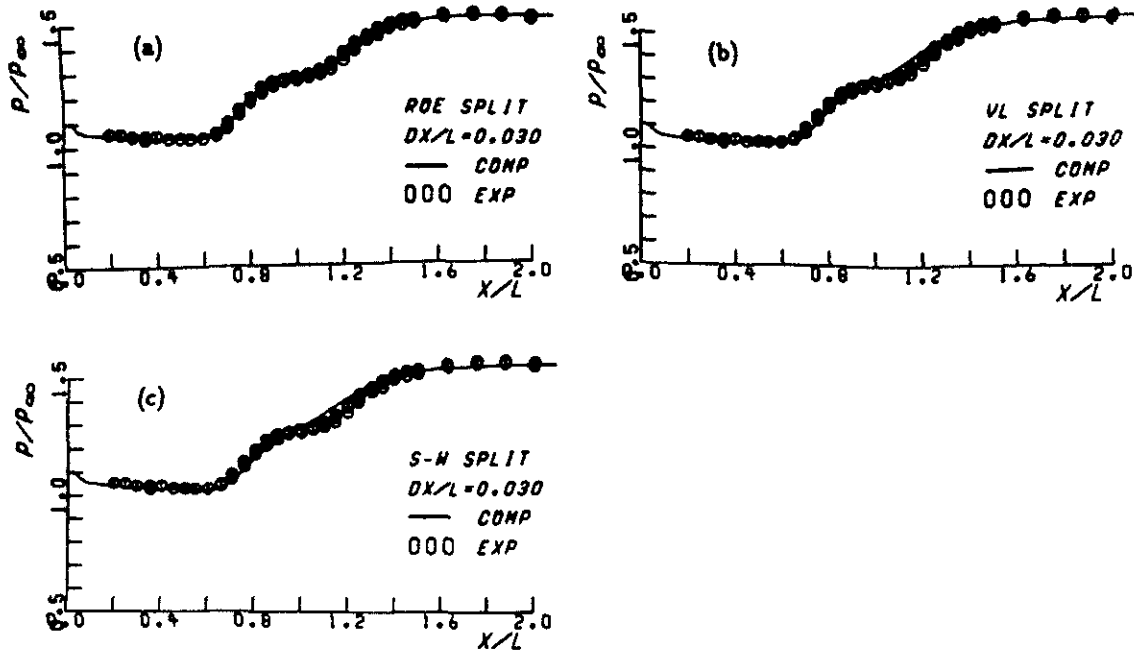
Figure 8. Surface pressure distribution P/P_∞ for a shock-wave/laminar boundary-layer interaction, $M_\infty = 2.2$, $Re_\infty = 1.0 \times 10^5$ and $\beta = 30.027°$; second-order accurate R(U) using (a) RS, (b) VLS and (c) SWS; symbols: measurement[20], solid line: computation.